

Assembling of Topological Defects at Neck-Shaped Membrane Parts

Pavlo Kurioz, Luka Mesarec, Aleš Iglič, and Samo Kralj*

The impact of intrinsic and extrinsic curvature on the distribution of topological defects (TDs) in neck-like regions of biological membranes is studied quantitatively. Biological membranes are modeled effectively at the mesoscopic level as two-dimensional films described in terms of the tensor nematic order parameter field and curvature fields. It is demonstrated that *antidefects* robustly form at the neck area and can promote a membrane fission. The assembling of *antidefects* near the catenoid's equatorial ring, where catenoids roughly mimic neck shapes are analyzed in more detail. It is demonstrated that for sufficiently strong curvatures, the effective topological charge Δm_{eff} within a strongly curved region equals zero, and the resulting structures are *topologically neutral*. Consequently, the total charge of *antidefects* within the region equals $\Delta m = -\Delta m_{\text{V}} - \Delta m_{\text{K}}$. In most cases, the positions of *antidefects* are strongly influenced by the extrinsic curvature.

field of the membrane.^[1–5] The dynamic evolution and static properties of these structures could be strongly influenced by topological defects (TDs),^[6,7] which inevitably form if some kind of in-plane ordering is present^[1,8] in membranes with a spherical topology. TDs introduce localized inhomogeneities in ordering that could weaken the local membrane structure. At the center of TDs, the in-plane order is ill-defined, and consequently, it is essentially melted. These “weaker” ordered regions could nucleate diverse membrane processes in general.^[4,8]

Membrane parts exhibiting neck-like shapes could be formed due to different mechanisms. For example, they could be triggered by local clustering of multicomponent proteins coats and rafts.^[2] These membrane parts impose an inherent curvature preference, which might cause

budding of closed membranes.^[2,3,9,10] Curvature generation in cellular membranes plays an important role in many different biological functions, such as trafficking, fission, fusion, and three-dimensional (3D) organization (e.g., caveolae).^[9,11] An example of protein-induced membrane bending is clathrin-mediated endocytosis, in which a multicomponent protein bends the membrane into a budded state.^[9] On the other hand, the dynamin family proteins play an important role in the membrane fission process in mammalian endocytosis.^[12] Budding of membranes is crucial for the vesiculation process, which is important for membrane trafficking, i.e., the movement of proteins, pathogens and other macromolecules. Furthermore, amphiphilic compounds may induce either membrane exvaginations (echinocytosis, spiculation), including budding and release of small exovesicles in human erythrocytes, or they could induce pronounced membrane invaginations (stomatocytosis).^[3] Budding processes might also be driven by accumulation and orientational ordering of anisotropic membrane components in the neck between the bud and the parent membrane.^[1,2] The effects of the membrane curvature on the orientation of anisotropic (deviatoric) membrane inclusions were studied in ref. [1]. The results showed that the free energy of anisotropic inclusions sharply decreased when the neck becomes narrow. Some anisotropic membrane inclusions may therefore stabilize the shape where the cell and the exovesicle are connected by a narrow neck. Furthermore, the budding process may occur due to a local change in the area difference between the outer and inner lipid layer^[13] or by a constriction force that pinches the membrane into a budded shape.^[10] In addition, the formation of

1. Introduction

Numerous membrane processes require the formation of structures possessing local neck-like regions with in-plane ordering of anisotropic membrane components in the curvature

P. Kurioz
Jožef Stefan International Postgraduate School
Jamova 39, 1000 Ljubljana, Slovenia

L. Mesarec, Prof. A. Iglič
Laboratory of Biophysics
Faculty of Electrical Engineering
University of Ljubljana
Tržaška 25, 1000 Ljubljana, Slovenia

Prof. A. Iglič
Laboratory of Clinical Biophysics
Faculty of Medicine
University of Ljubljana
Zaloška 9, 1000 Ljubljana, Slovenia

Prof. S. Kralj
Condensed Matter Physics Department
Jožef Stefan Institute
Jamova 39, 1000 Ljubljana, Slovenia
E-mail: samo.kralj@um.si

Prof. S. Kralj
Faculty of Natural Sciences and Mathematics
University of Maribor
Koroška 160, 2000 Maribor, Slovenia

 The ORCID identification number(s) for the author(s) of this article can be found under <https://doi.org/10.1002/pssa.201800722>.

DOI: 10.1002/pssa.201800722

neck-like membrane structures is an integral part of fusion and fission in cellular membranes.^[9,14]

Local neck structures are well modeled by catenoid geometries in several cases.^[14] These geometric shapes exhibit zero mean curvature and negative Gaussian curvature, representing minimal surfaces. The relationship between Gaussian curvature, spontaneous curvature, and neck geometry was studied in ref. [14]. The Helfrich model^[15] for lipid bilayers was used to determine the spontaneous curvature field stabilizing a catenoid-like membrane neck. They found that the spontaneous curvature field depends on the Gaussian curvature and that the catenoid-shaped neck has an energy barrier at a critical neck radius, which corresponds to the switch in the sign of the spontaneous curvature.^[14] Furthermore, narrow and highly curved fusion pores may be facilitated by accumulation of anisotropic membrane components with orientational ordering.^[1,2] The research indicated that topological defects in the region of the fusion pore may disrupt the fusion of the vesicle with the membrane.^[16] On the other hand, the fusion pore may also become completely opened in the process of full fusion of the vesicle with the membrane.^[16]

Membrane fission, which enables separation of membrane compartments into smaller volumes, is essential for cellular life. Membrane fission is required for many cellular functions, e.g., mitochondrial division,^[17,18] cytokinesis,^[19,20] viral egress,^[21] and generation of the endoplasmic reticulum network.^[22,23] The processes of membrane budding, fission, and fusion are essential mechanisms for membrane traffic, i.e., the transport of nutrients and waste.^[24,25] In the trafficking process, membrane-bound transport vesicles are the carriers of the cargo. This transport can take place within the cell (between different organelles) or across the cell membrane.^[26] Movement of cargo from the plasma membrane into the cell is referred to as endocytosis, whereas movement of cargo out of the cell is called exocytosis.^[26] In these processes, transport vesicles bud off from one membrane and can fuse with other membranes.^[26] It was established that a substantial increase of the membrane spontaneous curvature is a key requirement for the membrane fission. Spontaneous curvature can be increased by perturbations that generate a difference in area between membrane leaflets.^[27] In cells, an increase in the membrane spontaneous curvature required to drive the fission process could arise from protein–lipid interactions.^[28] Membrane fission might be facilitated by proteins with specific structural features, including helical scaffolds, constricting rings, and hydrophobic membrane insertions.^[29–31]

In contrast, a recent study reported a membrane fission mechanism that is independent of protein structure.^[28] This mechanism takes into account random collisions among crowded proteins, which generate substantial pressure that can dramatically increase the membrane curvature. Such pressure can stretch, bend, and ultimately disrupt the membrane surface, leading to fission.^[28] Membrane fission can also be explained by the effect of the area-difference elasticity and by the effects of coupling local lipid composition to the Gaussian curvature.^[25,32,33] A better understanding of the mechanisms of membrane budding and vesiculation is important for cancer research.^[34] Nanovesicles that are pinched off from cancer cells constitute cell-to-cell communication

systems. It has been indicated that nanovesicles can induce metastases from the primary tumor in this way. Therefore, they can be considered potentially relevant biomarkers for the prognosis, diagnosis, and treatment of cancer.^[34]

In this paper, we analyze the assembling of TDs at neck regions where they could, for example, trigger membrane fission. In the main part of the study, we approximate the neck shape by catenoid geometry.^[35] In particular, we study the impact of both the intrinsic and extrinsic curvature^[36,37] as well as the presence of specific impurities for assembling TDs in order to demonstrate the rich variety of possible TD configurations. However, in all cases, TDs remain localized relatively close to the region and exhibit minimal negative Gaussian curvature. We use simple mesoscopic modeling where we restrict the cases to those exhibiting nematic-type ordering.

2. Theoretical Background

We model membranes as thin two-dimensional (2D) films exhibiting an in-plane nematic liquid crystal order.^[7,8] We describe the membrane structure in terms of the curvature field and nematic order parameter field, and the details are given in ref. [38]. Here, we summarize only the key assumptions of the modeling.

2.1. Variational Fields

Curvature of a local membrane surface patch, which corresponds to a point at the mesoscopic scale, is characterized by the curvature tensor field^[1,15,34]

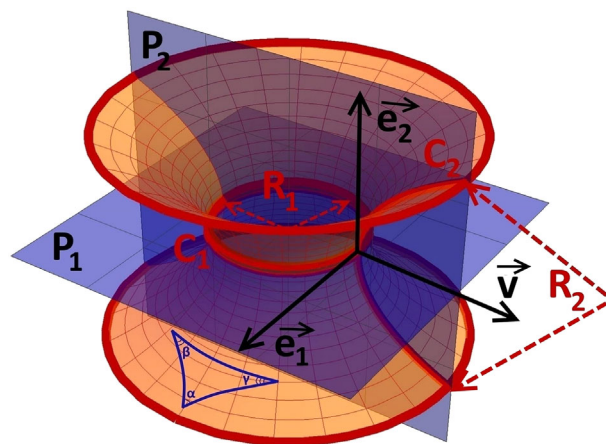


Figure 1. Schematic representation of a catenoid surface. A catenoid is a negatively curved (the sum of the interior angles of the geodesic triangle equals $\alpha + \beta + \gamma < \pi$) minimal surface ($H = 0$). The unit vectors \mathbf{e}_1 and \mathbf{e}_2 define the principal directions; \mathbf{v} indicates a surface unit normal vector. The blue planes P_1 , P_2 visualize the planes of principal curvatures in the meridional and equatorial directions. The intersection of the planes with the surface (red lines) forms the principal curvatures: $C_1 = \frac{1}{R_1}$, $C_2 = \frac{1}{R_2}$, where R_1 and R_2 are principal curvature radii.

$$\underline{C} = C_1 \mathbf{e}_1 \otimes \mathbf{e}_1 + C_2 \mathbf{e}_2 \otimes \mathbf{e}_2 \quad (1)$$

The unit vectors $\{\mathbf{e}_1, \mathbf{e}_2\}$ point along the surface principal directions with principal curvatures $\{C_1, C_2\}$, where $\mathbf{v} = \mathbf{e}_1 \times \mathbf{e}_2$ is the local surface normal. These quantities are illustrated in **Figure 1** for a case of catenoid geometry. The invariants of \underline{C} are the Gaussian curvature $K = C_1 C_2$ and the mean curvature $H = \frac{1}{2}(C_1 + C_2)$. Alternatively, the invariants of \underline{C} can also be curvature deviator D and mean curvature H , where $D^2 = H^2 - K$.^[1,34] The local nematic orientational order is described by the traceless and symmetric tensor order parameter field^[39]

$$\underline{Q} = q_1(\mathbf{e}_1 \otimes \mathbf{e}_1 - \mathbf{e}_2 \otimes \mathbf{e}_2) + q_2(\mathbf{e}_1 \otimes \mathbf{e}_2 + \mathbf{e}_2 \otimes \mathbf{e}_1) \quad (2)$$

where q_1 and q_2 are scalars. The nematic order parameter, which corresponds to the positive eigenvalue of \underline{Q} , is given by^[39]

$$\lambda = \sqrt{q_1^2 + q_2^2} \quad (3)$$

The corresponding unit eigenvector \mathbf{n} defines the local nematic order and is commonly referred to as the nematic director field. Note that at the origin of defects \mathbf{n} is not uniquely defined and consequently $\lambda = 0$.

2.2. Effective Topological Charge Cancellation Mechanism

The position and assembling of TDs can be estimated well by the effective charge cancellation mechanism (ETCC) for several

cases.^[38] ETCC embodies a well-known fact^[40,41] that Gaussian curvature acts like a smeared topological charge, i.e., patches exhibiting $K > 0$ ($K < 0$) attract TDs with a positive (negative) winding number m .^[7]

The ETCC mechanism reveals the preferred assembling tendency of TDs on surfaces exhibiting spatially varying K . One allocates to a surface patch $\Delta\zeta$ its spatially averaged characteristic Gaussian curvature \bar{K}

$$\bar{K} = \frac{1}{\Delta\zeta} \iint_{\Delta\zeta} K d^2\mathbf{r} \quad (4)$$

and its effective topological charge

$$\Delta m_{\text{eff}} = \Delta m + \Delta m_V + \Delta m_K \quad (5)$$

Here, Δm determines the total topological charge of the existing “real” TDs. Note that one commonly refers to TDs with $m > 0$ and $m < 0$ as *defects* and *antidefects*, respectively. Δm_V describes the “virtual” topological charge introduced by some “impurity” in the system that produced the same nematic director profile as a defect with a topological charge $m = \Delta m_V$. The spread topological charge is defined as^[38,40,41]

$$\Delta m_K = -\frac{1}{2\pi} \int_{\Delta\zeta} K d^2\mathbf{r} \quad (6)$$

The ETCC mechanism claims that each surface patch tends to be *topologically neutral*, i.e., Δm_{eff} tends to be zero. This can be

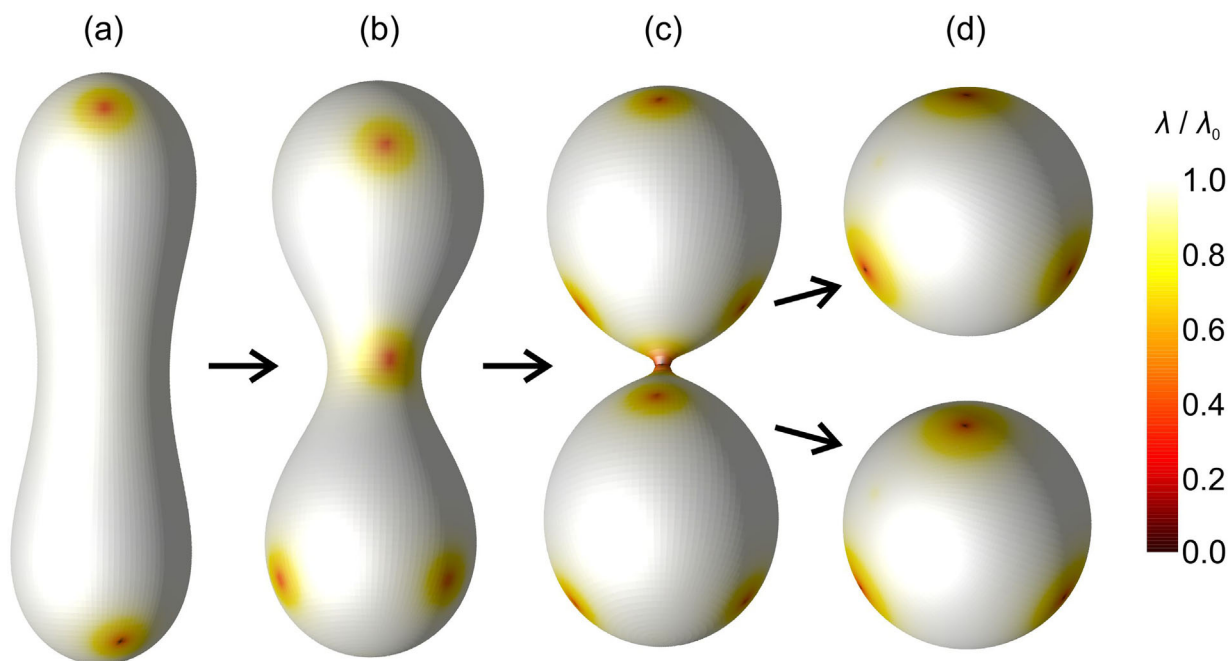


Figure 2. Equilibrium nematic ordering configurations calculated for different closed membrane shapes. Different shapes were obtained by varying the value of the spontaneous curvature of the membrane: (a) $C_0 = 0$, (b) $C_0 = 2$ and (c) $C_0 = 4$, where C_0 is measured in units $1/R$. For (a)–(c), the parameters were set to: $\nu = 0.70$, $R/\xi = 14$, $k_e^{(1)} = k_e^{(2)} = 0$, $k_i \ll \kappa$. The order parameter correlation length ξ estimates the core size of TDs, and λ_0 determines the equilibrium value of the order parameter in the limit $R \rightarrow \infty$. Spherical shapes in (d) were formed as a result of decomposition of the membrane in (c).

realized by redistribution of existing TDs or by creation of additional pairs $\{\text{defect}, \text{antidefect}\}$, and the details are given in ref. [38].

Note that the ETCC mechanism reveals the tendency of a system. Topologically neutral configurations could be relatively easily realized if they can be reached through redistribution of existing TDs. In cases that additional TDs are needed, then local regions exhibiting strong enough elastic distortions must be present to form nuclear pairs (*defect, antidefect*).

2.3. Free Energy Functional

We express the free energy as the sum $f = f_H + f_C + f_e^{(\text{int})} + f_e^{(\text{ext})}$ of Helfrich bending (f_H), nematic condensation (f_C), intrinsic elastic ($f_e^{(\text{int})}$), and extrinsic elastic ($f_e^{(\text{ext})}$) contributions, where

$$f_H = \frac{\kappa}{2}(C_1 + C_2 - C_0)^2 \quad (7a)$$

$$f_c = -a\text{Tr}(\underline{Q}^2) + b(\text{Tr}(\underline{Q}^2))^2 \quad (7b)$$

$$f_e^{(\text{int})} = k_i \text{Tr}(\nabla_s \underline{Q})^2 \quad (7c)$$

$$f_e^{(\text{ext})} = k_e^{(1)} \text{Tr}(\underline{Q}\underline{C})^2 + k_e^{(2)} \text{Tr}(\underline{C}^2 \underline{Q}^2) \quad (7d)$$

The parameters entering Equation (7) are the following. κ is the membrane bending modulus and C_0 the spontaneous curvature of the membrane surface.^[15] a and b are positive material constants in nematic phase, k_i is the intrinsic elastic modulus, ∇_s stands for the surface gradient operator,^[39] and $\{k_e^{(1)}, k_e^{(2)}\}$ are extrinsic elastic constants.^[35] Note that the contribution $\text{Tr}(\underline{Q}\underline{C}^2) \propto C_1^2 - C_2^2$ equals zero for the catenoid geometry, for which it holds $C_1 = -C_2$. Therefore, in our study, only the contribution weighted by $k_e^{(2)}$ is relevant.

In our simulations, we first consider the case where both tensor fields \underline{C} and \underline{Q} are variational parameters. In this case, we neglect the impact of extrinsic curvature and we treat pure systems (i.e., without “impurities” carrying $\Delta m_V \neq 0$). We study closed axisymmetric shapes exhibiting inversion symmetry. In the Cartesian coordinates (e_x, e_y, e_z) , the position vector of a generic point on an axisymmetric surface is determined by^[5,38]

$$\mathbf{r} = \rho(s)\cos(u)\mathbf{e}_x + \rho(s)\sin(u)\mathbf{e}_y + z(s)\mathbf{e}_z \quad (8)$$

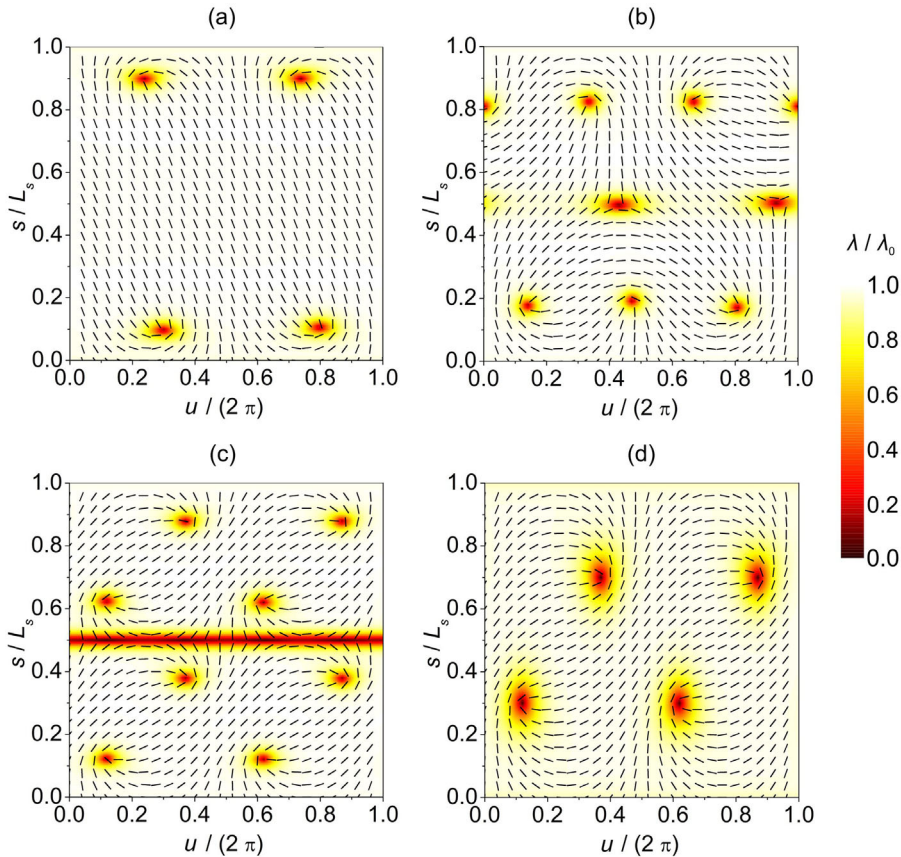


Figure 3. The degree of nematic ordering and superimposed nematic director field in the (u, s) -plane for the shapes presented in Figure 2.

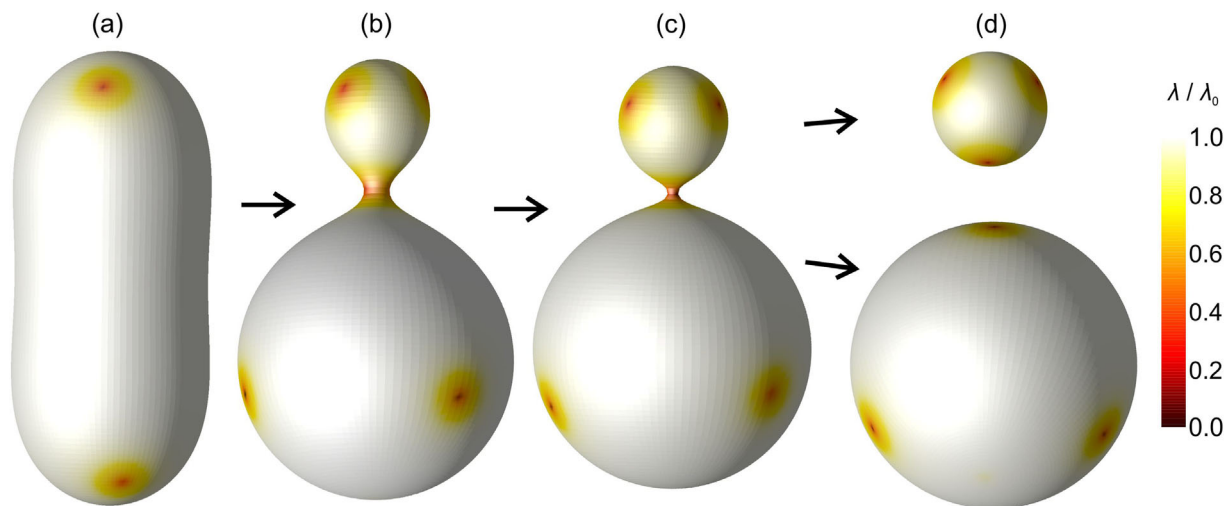


Figure 4. Equilibrium nematic ordering configurations calculated for different closed membrane shapes. Different shapes were obtained by varying the value of the spontaneous curvature of the membrane: (a) $C_0 = 0$, (b) $C_0 = 2$ and (c) $C_0 = 4$, where C_0 is measured in units $1/R$. For (a)–(c), the parameters were set to $\nu = 0.85$, $R/\xi = 14$, $k_e^{(1)} = k_e^{(2)} = 0$, $k_i \ll \kappa$. Spherical shapes in (d) were formed as a result of decomposition of the membrane in (c).

Here $\rho(s)$ and $z(s)$ are variational parameters defining the profile curve in the (x, z) -plane, s stands for the arc length of the profile curve, and u is the azimuthal angle. Equilibrium configurations are obtained by minimizing the total free energy

(Equation (7)) for fixed values of membrane surface and volume, and the details are given in refs. [38,42,43].

Next, we confine our interest to the impact of extrinsic curvature and “impurities.” In these simulations, we study the

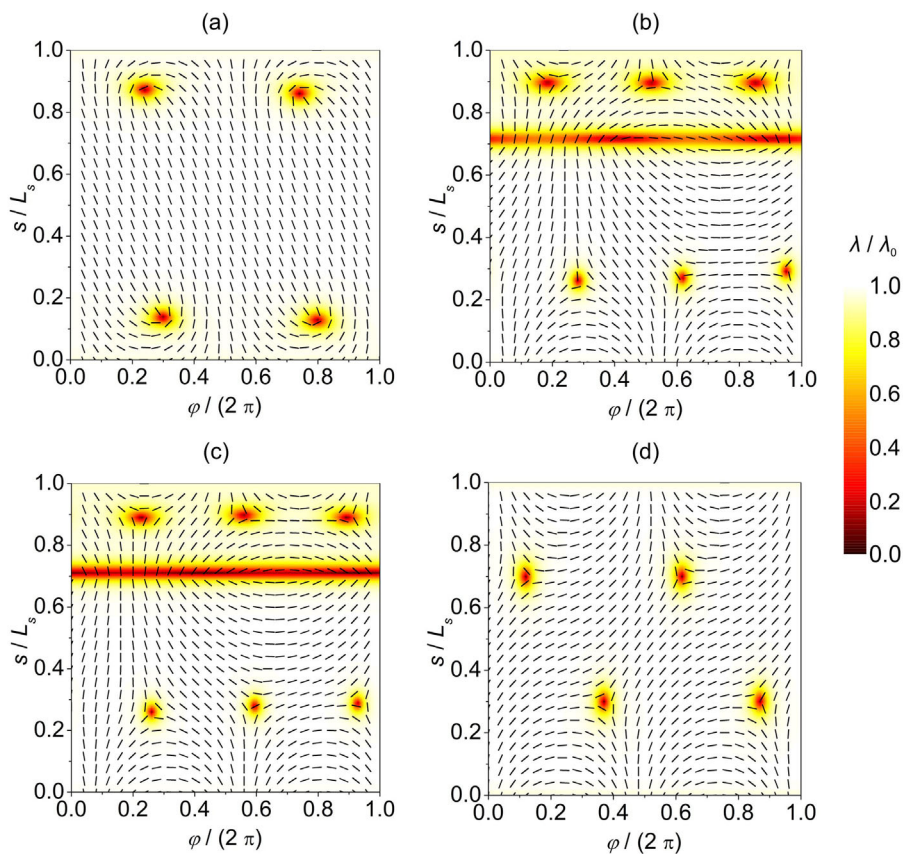


Figure 5. The degree of nematic ordering and superimposed nematic director field in the (u, s) -plane for the shapes presented in Figure 4.

degree of ordering for a given catenoid geometry. Therefore, only Q is a variational parameter while the curvature field is imposed. The catenoid shapes are defined by $\rho(s) = R_1 \cosh(s/R_1)$ and $z(s) = s$. An additional important length entering the modeling is the order parameter correlation length, which we define as $\xi = (a/k_i)^{1/2}$. It estimates the linear core size of defects well.

3. Results and Discussion

Our aim is to understand which parameters are the key parameters influencing the assembling of TDs at neck-like membrane structures and how they act. For this purpose, we first analyze the conditions under which topological defect-driven membrane fission is expected to occur. In the simulations, we let both curvature field and orientational field serve as variational parameters. In this analysis, we took only the intrinsic curvature term into account.

One “natural” parameter that can robustly trigger neck formation is the reduced volume $v = V/V_0$. Here, V stands for the volume of the shape, and $V_0 = 4\pi R^3/3$ is the volume of a spherical surface of the same surface area A and radius $R = \sqrt{A/(4\pi)}$.^[44] All lengths in our model are scaled with respect to R , which represents a typical linear dimension of the

shape. Our model is applicable for membrane shapes with different length scales. The typical diameter of lipid vesicles is 30–50 nm for small unilamellar vesicles (SUVs), 100–200 nm for large unilamellar vesicles (LUVs), and up to 100 μm for giant unilamellar vesicles (GUVs),^[45] whereas the typical diameter of cells ranges from 0.1 to 25 μm . For example, in experiments with giant phospholipid vesicle of typical diameter $\approx 10 \mu\text{m}$, a tubular bud with a diameter of $\approx 1 \mu\text{m}$ was formed. This bud detached itself from the mother vesicle and decomposed into separate spherical vesicles with $\approx 1\text{-}\mu\text{m}$ diameters. Before the separation, these vesicles were connected by thin necks with diameters of $\approx 50 \text{ nm}$.^[46] On the other hand, the typical diameter of a spherical bud at the top of an echinocyte spicule is $\approx 50 \text{ nm}$ with a neck diameter $\approx 25 \text{ nm}$.^[47] Our dimensionless model can be used for systems of any length scale. Nevertheless, the effects of orientational ordering were most profound at smaller length scales, i.e., at higher curvatures. In our simulations, we assume that a closed membrane shape undergoes a shape transformation from a prolate shape (Figure 2a) to the shape with a thin neck (Figure 2c). The neck region of the closed membrane shape resembles a catenoid surface (Figure 2b and c). This transformation is enabled by increasing the value of the spontaneous curvature of the membrane C_0 (see Equation (7) a). The structural change happens relatively abruptly at the

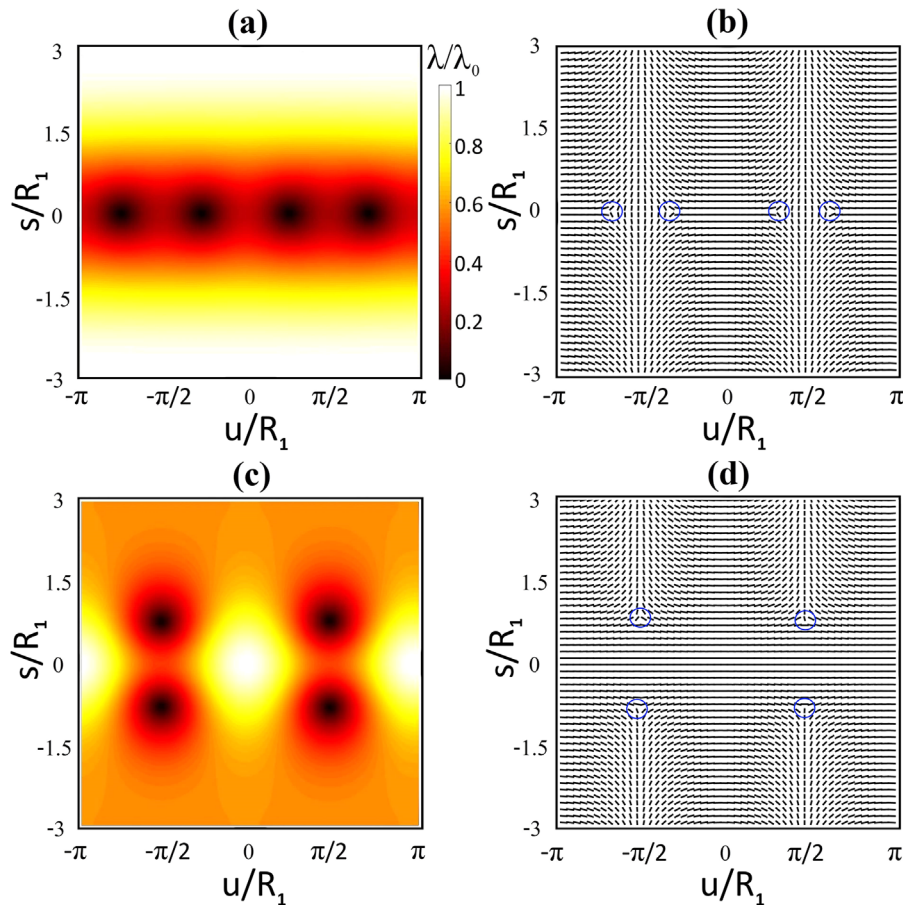


Figure 6. 2D Plots of the order parameter (left panel) and the director field (right panel) with decreases in the extrinsic elastic constant $k_e^{(2)}$: (a and b) $k_e^{(2)}/k_i = 0.0$, (c and d) $k_e^{(2)}/k_i = -2.4$, $R_1/\xi = 0.5$. The locations of TDs are marked with blue circles in (b) and (d).

critical value of C_0 . Note that the spontaneous curvature is correlated to the curvature preferred by the membrane. In our simulations, C_0 is scaled with respect to R . Therefore, increasing C_0 can be interpreted as increasing the size of the closed membrane shape at the constant value of the nonscaled C_0 . With increasing C_0 , we therefore simulate membrane growth.

In **Figure 3**, ordering amplitude and director field are shown in the (u, s) plane where the positions of topological defects are clearly visible. Here, s stands for the arc length of the profile curve of the shape. The profile curve of the length L_S is rotated around the z -axis by an angle of $u = 2\pi$ to obtain the closed axisymmetric membrane shape of spherical topology. According to the Gauss–Bonnet and Poincaré–Hopf theorems,^[48] topological defects are unavoidably formed on closed surfaces with spherical topology, where the total topological charge is given by $m_{\text{tot}} = 2$.^[7] Prolate shape (**Figure 2a** and **3a**) hosts four $m = 1/2$ topological defects, which are attracted toward the poles, where Gaussian curvature has the highest value. Because of their mutual repulsion, topological defects are not located exactly at the poles. On increasing the spontaneous curvature C_0 of the membrane, the neck becomes thinner (**Figure 2b**). Gaussian curvature is negative at the neck and positive on the rest of the

membrane surface, which triggers the formation of two new defect-antidefect pairs (**Figure 2b** and **3b**). Note that in this case, the surface patches of the structure are only partially *neutralized* (i.e., complete neutralization would require eight $m = 1/2$ defects in the spherical part and four $m = -1/2$ antidefects in the neck). The shape in **Figure 2b** therefore hosts six defects and two antidefects. After increasing C_0 , the neck becomes even thinner (**Figure 2c**). The catenoid-like neck region now separates two, almost spherical parts of the membrane (**Figure 2c**) if the total free energy of the resulting two-object structure is lower. Fission could be enabled in practice by the presence of TDs. Due to relatively strong orientational fluctuations, the effective interaction between the neighboring molecules is sufficiently weakened to trigger the decay.

In the example above, we set $\nu = 0.7$. **Figure 4** and **5** present a similar process where $\nu = 0.85$. In this case, the up-down mirror symmetry is broken with varying C_0 . Furthermore, in this case, the intermediate defect structures are different.

We next analyze the various defect structures at the neck area in more detail with varying material (i.e., values of elastic moduli) properties and geometrical details. For this purpose, we mimic the neck-like shape formed by catenoids. Therefore, we

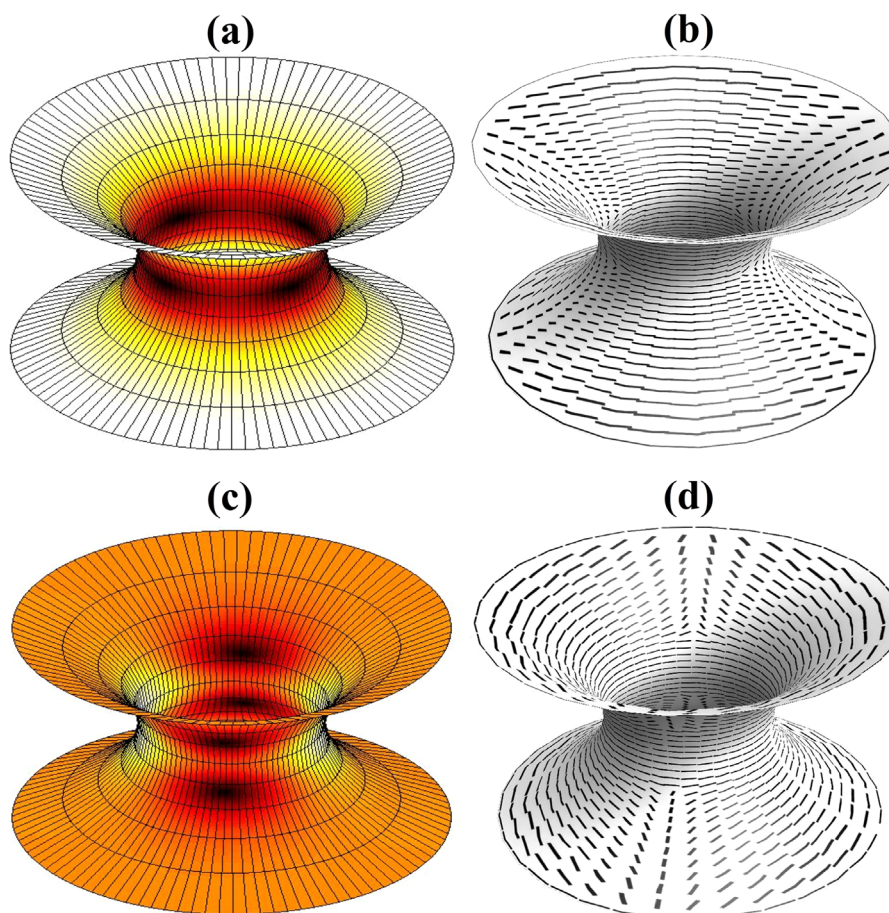


Figure 7. Nematic textures on catenoidal shells with variations in the extrinsic curvature strength. The corresponding order parameter and director field profiles in plane (u, s) are depicted in **Figure 6**.

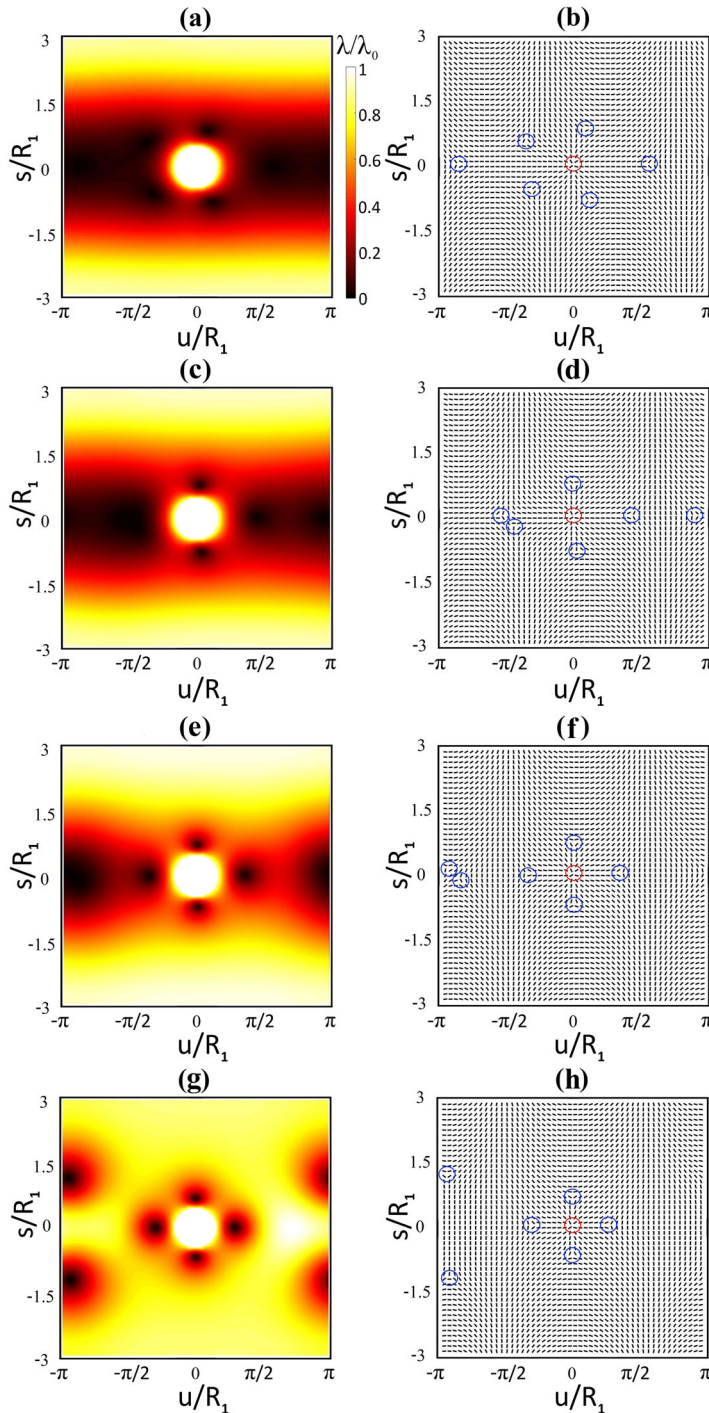


Figure 8. Calculated order parameter and the director field profiles in (u, s) plane of the catenoid in the presence of a fixed “impurity” with varying $k_e^{(2)}$. The order parameter and director field variations are shown in the left and right columns, respectively. The fixed circular NP of the radius $r = \xi$ is placed at $(u_{NP} = 0, s_{NP} = 0)$. The NP effectively acts as a TD bearing $m_V = 1$. Textures are obtained for (a and b): $k_e^{(2)} = 0$, (c and d): $k_e^{(2)} = -1$, (e and f): $k_e^{(2)} = -2$, (g and h): $k_e^{(2)} = -2.4$, $R_1/\xi = 0.5$. The locations of TDs are marked with blue circles, and the nanoparticle is marked with the red circle.

prescribe the shape of the films and focus solely on the impact of elastic properties on distribution of TDs in the neck area. Note that according to the ETCC mechanism, the defects bearing a negative topological charge will accumulate at the neck area. However, their exact positioning there can generally be strongly influenced by the relative strength of extrinsic and extrinsic elastic terms. We refer to the narrowest region of a catenoid as the *equatorial ring* of radius R_1 (see Figure 1). In simulations, we vary R_1 and the ratio $\mu = k_e^{(2)}/k_i$. We also demonstrate the impact of “impurities” on the patterns of TDs. For this purpose, we insert circular objects of the radius $r = \xi$, which locally enforce either $\Delta m_V = 1$ or $\Delta m_V = -1$ (see Equation (5)). Such conditions could be realized, e.g., by introducing an appropriately surface-treated nanoparticle.^[49]

In all cases, we consider catenoids possessing small enough R_1 (i.e., comparable to ξ), so that TDs are generated. Note that for $R_1 \gg \xi$, there are no defects. For thin enough *equatorial rings*, TDs that are created via $\{\text{defect, antidefect}\} = \{m = 1/2, m = -1/2\}$ pair formation appear. The *antidefects* are attracted to the *equatorial ring* where negative Gaussian curvature exhibits a minimum. The *defects* are expelled outside catenoids, which is enabled in our simulations by the imposed free boundary condition. Furthermore, for catenoids, it holds $\Delta m_K(\Delta \zeta) = 2^{[35]}$ (see Equation (4)), where the surface patch $\Delta \zeta$ determines the catenoid’s part exhibiting a relatively strong curvature. In Figure 6 and 7, we demonstrate the impact of μ on the distribution of TDs in the absence of “impurities.” In all cases, four $m = -1/2$ are present. Consequently, the structures are *topologically neutral* (i.e., $\Delta m_{\text{eff}} = 0$). For $\mu = 0$, the effective *extrinsic ordering field* is absent. TDs are assembled at the equatorial ring where the Gaussian curvature exhibits the minimal value. On increasing μ , the relative importance of the extrinsic curvature term increases. The resulting *extrinsic ordering field* is strongest at the *equatorial ring* and then monotonously decreases when increasing the distance from the *ring*. For a large enough value of $k_e^{(2)}$, TDs are expelled from the *ring*, as shown in Figure 6(c and d) and 7(c and d).

In Figure 8, we analyze the case where a fixed “impurity” enforcing $\Delta m_V = 1$ is placed within the *ring*. In this case, six $m = -1/2$ TDs exist, which correspond to topologically neutral structures. After increasing μ , the defects redistribute. However, even for relatively large values of $k_e^{(2)}$, two $m = -1/2$ *antidefects* remain localized on the *ring* because they are strongly pinned to the “impurity.”

Finally, in Figure 9, we consider a case where fixed “impurity” enforces $\Delta m_V = -1$. In this case, two $m = -1/2$ *antidefects* are introduced, and the resulting structures are therefore *topologically neutral*. Note that on increasing $k_e^{(2)}$, the pattern of TDs does not display qualitative changes.

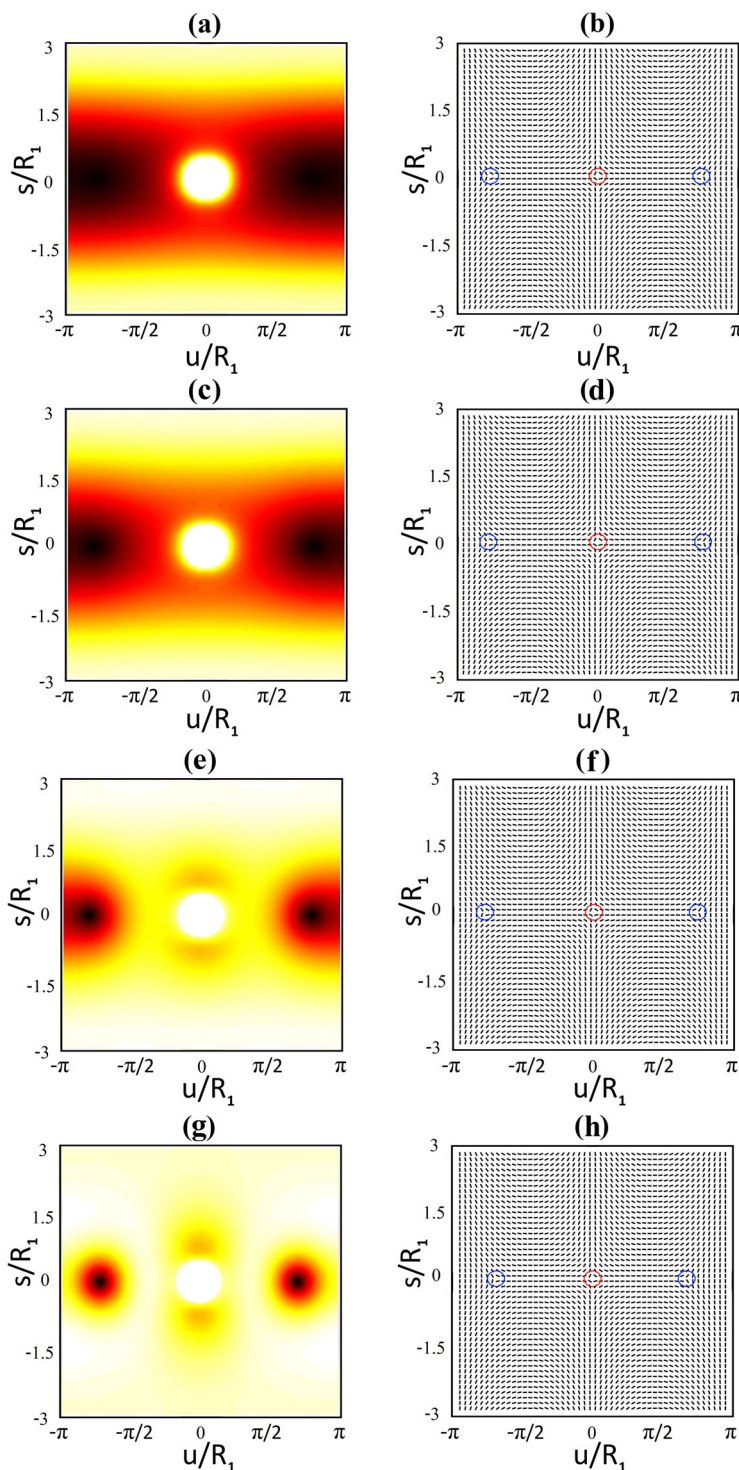


Figure 9. Calculated order parameter and the director field profiles in the (u, s) plane of the catenoid in the presence of an “impurity” imposing $m_V = -1$ on variations in $k_e^{(2)}$. The order parameter and director field variations are shown in the left and right columns, respectively. The fixed circular NP of the radius is placed at $(u_{NP} = 0, s_{NP} = 0)$. The NP effectively acts as a TD bearing $m_V = -1$. Textures are obtained for (a and b): $k_e^{(2)} = 0$, (c and d): $k_e^{(2)} = -1$, (e and f): $k_e^{(2)} = -2$, (g and h): $k_e^{(2)} = -2.4$, $R_1/\xi = 0.5$. The locations of TDs are marked with blue circles, and the nanoparticle is marked with the red circle.

4. Conclusions

We quantitatively studied the patterns of TDs in thin nematic films with regions exhibiting neck-like shape. Such systems, among others, roughly mimic biological membranes exhibiting in-plane ordering. These membranes are often present either due to the anisotropic structure of membrane constituents or due to attached anisotropic nano-objects. In the modeling, we used a Helfrich-Landau-de Gennes type mesoscopic approach in terms of the curvature tensor field and nematic tensor order parameter field. We confined our studies to structures exhibiting axially symmetric shapes, for which we calculated nematic configurations that break this symmetry. We focused on number and positional assembling of TDs in orientational ordering.

We first demonstrated that in structures possessing neck-like areas, *antidefects* are likely to be assembled. These *antidefects* might trigger a membrane fission process by effectively weakening intermolecular interactions at the neck area. We then restricted our attention to the neck area and analyzed how material properties, such as intrinsic or extrinsic curvature and “impurities,” affect the number and positions of *antidefects*. For this purpose, we approximated the neck shape with catenoid geometry. Furthermore, we limited our studies to cases where “impurities” effectively act as local topological defects, which are characterized either by a virtual topological charge $\Delta m_V = 1$ or $\Delta m_V = -1$. Our simulations reveal that for strong-enough neck curvatures, which are expected in a typical fission process, several *antidefects* are robustly present within or near the *equatorial ring* of a neck. Specifically, variations of key model control parameters only affected the local spatial distribution of *antidefects*, which, however, remained localized within the *equatorial* area.

Note that in-plane membrane order could exhibit also other symmetries described, e.g., by vector or hexagonal order parameter field.^[40,41] For example, the vector (hexagonal) order parameter field allows minimal topological charges $m = \pm 1$ ($m = \pm 1/6$). In the case of an approximately spherical surface patch, one would need two (12) topological defects to form a *topologically neutral* patch. However, our analysis is at least qualitatively appropriate for such cases because key features rely on topology. The topology is insensitive to microscopic details, and several universal features emerge as a result.

Supporting Information

Supporting Information is available from the Wiley Online Library or from the author.

Acknowledgments

S.K. acknowledges the financial support from the Slovenian Research Agency (research core funding No. P1-0099). A.I. and

L.M. acknowledge the financial support from the grant No. P2-0232. Both grants were from the Slovenian Research Agency (ARRS).

Conflict of Interest

The authors declare no conflict of interest.

Keywords

membranes, minimal surfaces, nematic liquid crystals, topological defects, topology

Received: September 15, 2018

Revised: November 30, 2018

Published online:

-
- [1] V. Kralj-Iglič, V. Heinrich, S. Svetina, B. Žekš, *Eur. Phys. J. B* **1999**, 10, 5.
- [2] A. Iglič, B. Babnik, K. Bohinc, M. Fosnaric, H. Hagerstrand, V. Kralj-Iglič, *J. Biomech.* **2007**, 40, 579.
- [3] H. Hagerstrand, L. Mrówczyńska, U. Salzer, R. Prohaska, K. Michelsen, V. Kralj-Iglič, A. Iglič, *Mol. Memb. Biol.* **2006**, 23, 277.
- [4] D. Jesenek, Š. Perutkova, W. Gózd, V. Kralj-Iglic, A. Iglič, S. Kralj, *Nanomedicine* **2013**, 8, 677.
- [5] L. Mesarec, A. Iglič, S. Kralj, *Adv. Biomed. Res. Innov.* **2018**, 1, 1.
- [6] N. D. Mermin, *Rev. Mod. Phys.* **1979**, 51, 591.
- [7] M. V. Kurik, O. D. Lavrentovich, *Physics-Uspeski* **1988**, 31, 196.
- [8] F. C. MacKintosh, T. C. Lubensky, *Phys. Rev. Lett.* **1991**, 67, 1169.
- [9] M. Chabanon, J. C. Stachowiak, P. Rangamani, *WIREs Syst. Biol. Med.* **2017**, 9, e01386.
- [10] H. Alimohamadi, R. Vasan, J. Hassinger, J. Stachowiak, P. Rangamani, *Mol. Biol. Cell* **2018**, 29, 2024.
- [11] J. Zimmerberg, M. M. Kozlov, *Nat. Rev. Mol. Cell. Biol.* **2006**, 19, 7.
- [12] D. Loerke, M. Mettlen, D. Yarar, K. Jaqaman, H. Jaqaman, G. Danuser, S. L. Schmid, *PLoS Biol.* **2009**, 7, e1000057.
- [13] A. Iglič, H. Hagerstrand, *Med. Biol. Eng. Comput.* **1999**, 37, 125.
- [14] M. Chabanon, P. Rangamani, *Soft Matter* **2018**, 14, 2281.
- [15] W. Helfrich, *Z Naturforsch C.* **1973**, 28, 693.
- [16] D. Jesenek, Š. Perutkova, V. Kralj-Iglič, S. Kralj, A. Iglič, *Cell Calcium* **2012**, 52, 277.
- [17] J. A. Mears, L. L. Lackner, S. Fang, E. Ingerman, J. Nunnari, J. E. Hinshaw, *Nat. Struct. Mol. Biol.* **2011**, 26, 18.
- [18] C. Fröhlich, S. Grabiger, D. Schwefel, K. Faelber, E. Rosenbaum, J. Mears, O. Rocks, O. Daumke, *EMBO J.* **2013**, 32, 1280.
- [19] J. G. Carlton, J. Martin-Serrano, *Science* **2007**, 316, 1908.
- [20] E. Morita, V. Sandrin, H. Y. Chung, S. G. Morham, S. P. Gygi, C. P. Rodesch, W. Sundquist, *EMBO J.* **2007**, 26, 4215.
- [21] S. B. Van Engelenburg, *Science* **2014**, 343, 653.
- [22] J. Hu, Y. Shibata, P. P. Zhu, C. Voss, N. Rismanchi, W. A. Prinz, T. A. Rapoport, C. Blackstone, *Cell* **2009**, 138, 549.
- [23] C. Lee, L. B. Chen, *Cell* **1988**, 54, 37.
- [24] S. D. Conner, S. L. Schmid, *Nature* **2003**, 422, 37.
- [25] C. M. Chen, P. G. Higgs, F. C. MacKintosh, *Phys. Rev. Lett.* **1997**, 79, 1579.
- [26] J. M. Herrmann, A. Methods, *Mol. Biol.* **2015**, 1270, 1.
- [27] J. Sanborn, K. Oglecka, R. S. Kraut, A. N. Parikh, *Faraday Discuss.* **2013**, 161, 167.
- [28] W. T. Snead, C. C. Hayden, A. K. Gadok, C. Zhao, E. M. Lafer, P. Rangamani, J. C. Stachowiak, *Proc. Natl. Acad. Sci. USA* **2017**, 114, E3258.
- [29] O. Daumke, A. Roux, V. Haucke, *Cell* **2014**, 156, 882.
- [30] H. T. McMahon, J. L. Gallop, *Nature* **2005**, 438, 590.
- [31] F. Campelo, H. T. McMahon, M. M. Kozlov, *Biophys. J.* **2008**, 95, 2325.
- [32] L. Miao, U. Seifert, M. Wortis, H. G. Döbereiner, *Phys. Rev. E* **1994**, 49, 5389.
- [33] U. Seifert, *Adv. Phys.* **1995**, 46, 13.
- [34] V. Kralj-Iglič, *Int. J. Nanomed.* **2012**, 7, 3579.
- [35] B. L. Mbanda, G. M. Grason, C. D. Santangelo, *Phys. Rev. Lett.* **2012**, 108, 017801(1–5).
- [36] R. L. B. Selinger, A. Konya, A. Travesset, J. V. Selinger, *J. Phys. Chem. B* **2011**, 115, 13989.
- [37] G. Napoli, L. Vergori, *Phys. Rev. Lett* **2012**, 108, 207803(1–5).
- [38] L. Mesarec, W. Gózd, A. Iglič, S. Kralj, *Sci. Rep.* **2016**, 6, 27117(1–12).
- [39] S. Kralj, R. Rosso, E. G. Virga, *Soft Matter* **2011**, 7, 670.
- [40] V. Vitelli, A. M. Turner, *Phys. Rev. Lett.* **2004**, 93, 215301(1–4).
- [41] M. Bowick, D. R. Nelson, A. Travesset, *Phys. Rev. E* **2004**, 69, 041102(1–12).
- [42] W. Gózd, *Langmuir* **2004**, 20, 7385.
- [43] W. Gózd, *J. Phys. Chem. B* **2005**, 109, 21145.
- [44] L. Mesarec, W. Gózd, S. Kralj, M. Fosnaric, S. Penic, V. Kralj-Iglič, A. Iglič, *Eur. Biophys. J.* **2017**, 46, 705.
- [45] A. Iglič, D. Drobne, V. Kralj-Iglič, *Nanostructures in Biological Systems: Theory and Applications*. Pan Stanford, New York **2015**.
- [46] J. Urbanija, N. Tomšič, M. Lokar, A. Ambrožič, S. Čučnik, B. Rozman, V. Kralj-Iglič, *Chem. Phys. Lipids* **2007**, 150, 49.
- [47] V. Kralj-Iglič, A. Iglič, H. Hagerstrand, P. Peterlin, *Phys. Rev. E* **2000**, 61, 4230.
- [48] R. D. Kamien, *Rev. Mod. Phys.* **2002**, 74, 953.
- [49] G. Cordoyiannis, P. Losada-Pérez, Ch. Shekhar Pati Tripathi, B. Rožič, U. Tkalec, V. Tzitzios, E. Karatairi, G. Nounesis, Z. Kutnjak, I. Mušević, Ch. Glorieux, S. Kralj, J. Thoen, *Liq. Cryst.* **2010**, 37, 1419.